6.   Destriping of *FIRAS* Data

The *FIRAS* destriper, FMD, designed to correct for residual instrumental effects in the calibrated coadd spectra, is the facility which produces the pixel spectra and associated errors. If the calibration model does not sufficiently account for all the "sources" in the *FIRAS* instrument, the propagation of their effects into the calibrated spectra will produce discrepancies between different observations within the same sky pixel. The destriper attempts to model these as a set of offset (subtractive) correction spectra. Unlike the primary calibration program, the destriper uses both sky and calibration data, producing the correction spectra by minimizing the discrepancy between multiple observations within the same sky pixel for the former and deviations from a Planck (blackbody) spectrum for the latter. Also, unlike the primary calibration, the destriper is linear.

6.1.   Destriper Model

The destriper minimizes:

$$\chi^2 = \sum_i \left[S_i^{(sky)} - A_{p(i)} - \sum_k J_k f_{ki} \right]^2 w_i + \sum_i \left[S_i^{(cal)} - P_i - \sum_k J_k f_{ki} \right]^2 w_i \qquad (16)$$

with respect to A_p, the destriped spectrum for the pth sky pixel and J_k, the offset spectra for the kth correction. These quantities are computed independently for each frequency so we have suppressed the frequency index. $S_i^{(sky)}$ is the ith calibrated sky spectrum, $S_i^{(cal)}$ is the ith calibrated calibration spectrum, P_i is a Planck spectrum at the external calibrator (XCAL) temperature of the ith calibration observation, f_{ki} is the value of the kth model function for the ith sky or calibration observation and w_i is the corresponding effective weight for this observation. The first sum is over all sky observations, excluding those within pixels whose center is located within a mask of the Galactic center. The Galactic exclusion is made to minimize errors due to spatial gradients. The use of spatial gradient correction functions (Section 6.3.3) allows us to use more of the Galactic region in the destriper. Analysis of χ^2 as a function of Galactic coordinates showed that some masking is still needed. The Galactic masks selected are :

LOWF (freq < 630 GHz) : $[b < 5, l < 30]$
HIGH (600 GHz < freq) : $[b < 8, l < 100]$

The second sum is over the "cold-null" calibration spectra taken with all four major controllables, external calibrator (XCAL), internal calibrator (ICAL), sky horn (SKYH), and reference horn (REFH), set between 2.6 K and 2.8 K. The calibrated coadd spectra S_i

are acquired from the calibrated spectra records. The Planck spectra P_i are computed from the XCAL temperatures of the calibration observations. The A_p are the derived pixel spectra, with the offset corrections applied. To operate the destriper, it is necessary to determine the observation weights w_i and to select the model functions f_{ki} .

6.2.   Observation Weights

Ideally, the weight for each observation would be the inverse of its variance, which is calculated from the dispersions of the individual interferograms which make up the observation (Section 7.1.1) . In general, the measured variance of an observation deviates from the variance of the underlying process. The effect of using measured variances overweights those observations whose measured variance is smaller than its long term average variance. The destriper minimization fit then is incorrectly dominated by observations whose measured variances are much smaller than their long term average variances.

The solution is to derive a parametric model for the weights. The simplest model is to use the number of interferograms in the coadd as the weight, adopting the premise that all interferograms are equal. Since we know from theory and from our analysis of the data that the interferogram noise is dependent on the glitch rate, we have already incorporated a glitch rate correction into our model (Section 4.4 and Table 4.8).

Prior to deriving a final model for the weights, it is necessary to identify and eliminate any bad observations which have managed to elude the quality checks applied upstream in the pipeline, since they will corrupt the fit. The destriper is initially run for the 10 individual channels: the low resolution low frequency data sets LLSS, LLFA, RLSS, and RLFA; the high resolution low frequency data sets LLLF and RLLF; and the low resolution high frequency data sets LHSS, LHFA, RHSS, and RHFA. The initial weights are the weights determined at the coaddition stage. For each observation, the χ^2 combined over the entire frequency band is examined. Observations with anomalously high χ^2 per degree of freedom are identified and eliminated by having their weights set to zero.

The weights for each of the 10 individual channels are derived by fitting a parametric model to the measured variances of the surviving observations. Each individual channel is fitted with its own model. Model parameters include glitch rate, bolometer responsivity, ecliptic latitude, and time. Time dependences are modelled by a set of Legendre polynomials. The maximum order of the time polynomials is seven, capable of resolving time scales greater than 10 days. Variations on shorter time scales are modelled by a

running filter function of width three days or less. The selection of the optimum parametric model is made as follows. A trial model is applied to derive tentative observation weights. The destriper is run with the trial weights, and the χ^2 combined over the frequency band is computed for each observation from its dispersion from the pixel mean, for sky data, or its dispersion from a Planck spectrum, for calibration data. The distribution of combined χ^2 is fit to a theoretical distribution to determine the RMS scatter of the actual variance from the model variance. We iteratively converge on a model which minimizes the RMS scatter. The optimal model is then applied in production. Using this method, we are able to derive weights with an RMS error of 15% for low channel spectra and 8% for high channel spectra.

Note that we use a dimensionless weight, so that the expression minimized by our fit had dimensions of (*spectral intensity*)^2. Implicit in the model is a common variance, σ_ν, that applies to all observations and provides a scale for the χ^2. In fact, a variance is computed from the residual variation among multiple observations within the same pixel. The corresponding σ is called the *C-Vector* and is discussed in Section 7.1.

A few more steps are taken to determine the final set of observation weights. First, a more sensitive test for bad observations can be applied by screening out those with combined χ^2 per degree of freedom greater than a specified threshold. The destriper is run again with these observations de-weighted. The relative weights for the individual channel combinations are then derived from their *C-Vectors*. The destriper is run again for the combined data set. A final test for anomalous χ^2 per degree of freedom is made to screen out any remaining bad observations. Finally, the observation weights are scaled so that the total weight is equal to the number of sky pixels, so that the average total weight per pixel is one.

Table 6.1 gives the sky coverage for each data set and weight of an average IFG in each channel. Comparison with Table 5.4 shows the number of IFGs eliminated during the destriping process.

6.3.   Destriper Model Functions

We have broken the high frequency data into four frequency sections. The lowest section, (HI1), covers the same frequency range as the LOWF. After careful inspection we decided that the difficulty in correcting for the systematic effects in the low frequency end of the high frequency data exceeded the possible improvements to the LOWF data. The other 3 ranges (HI2, HI3, and HI4) were destriped separately with separate model functions. These were later rejoined to form the HIGH data set.

Table 6.1:   Number of IFGs and Relative IFG Weightings in Destriped *FIRAS* Skymaps

	LHSS	LHFA		RHSS	RHFA	
Number of pixels	5962	6002		5969	5999	
Number of IFGs	130784	169875		129595	170917	
IFG Weight*	0.998	0.265		35.201	9.491	
	LLSS	LLFA	LLLF	RLSS	RLFA	RLLF
Number of pixels	5960	5995	5899	5970	5993	5936
IFG Weight*	126591	157118	117944	126791	159461	122168
Obs/1000IFGs	32.250	4.161	38.165	9.952	1.279	11.743

*Weight per 1000 IFGs. The weight has been scaled so that the total weight of the entire dataset is equal to the number of pixels, 6144.

The art of destriping lies in the selection of the model functions f_{ki} . The set of model functions for previous releases of *FIRAS* data was limited to two exponentially decaying time functions and tophats corresponding to the entire mission period and those periods when the temperatures of the sky horn and reference horn were raised to 6K and 4K. The decaying exponentials were used to model an unidentified source of excess emission which was present at the start of the mission. With our improved sensitivity, additional correlates for the residuals were found, allowing us to expand our set of model functions.

6.3.1.   Special Time Period (Tophat) Functions

We use the same three tophat functions as in the previous releases of *FIRAS* data. One change has been to restrict their use to the frequency bands where they reduce χ^2 by a significant amount as measured by an F-statistic (Bevington 1969).

LOWF (freq < 630 GHz)	: [6K,4K,Mission]
HIF2 (600 GHz < freq < 1350 GHz)	: [6K,Mission]
HIF3 (1350 GHz < freq < 2100 GHz)	: [Mission]
HIF4 (2100 GHz < freq)	: [Mission]

Separate tophat corrections are computed for each of the individual channel combinations.
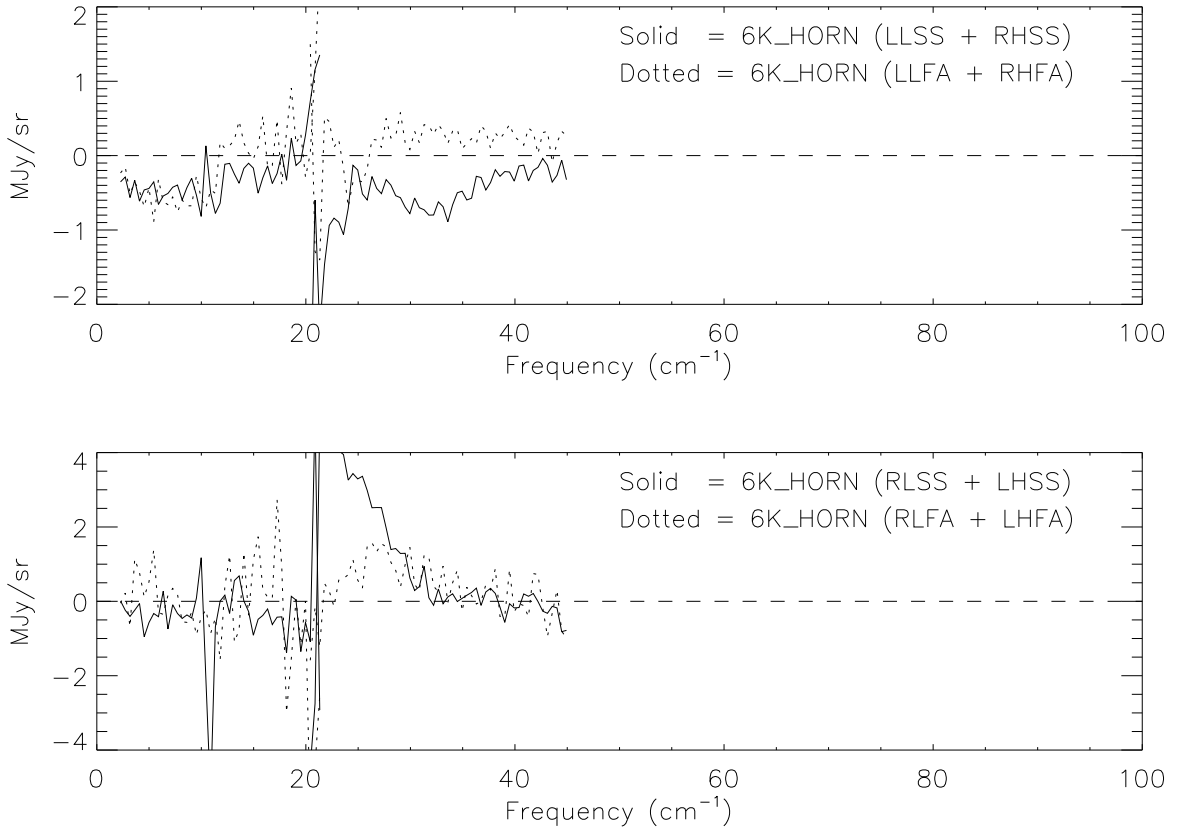
Fig. 6.1.— '6K Horn' offset correction spectra — Applied to the observations for the 6K horn period.
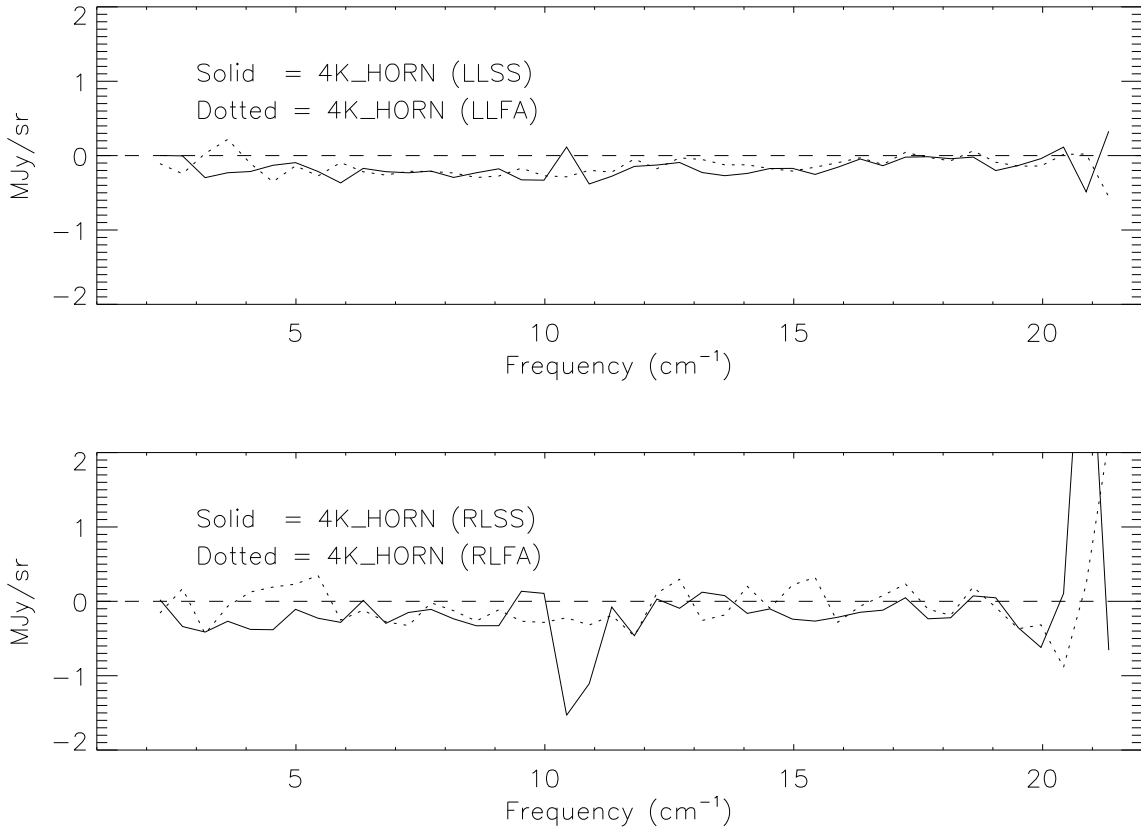
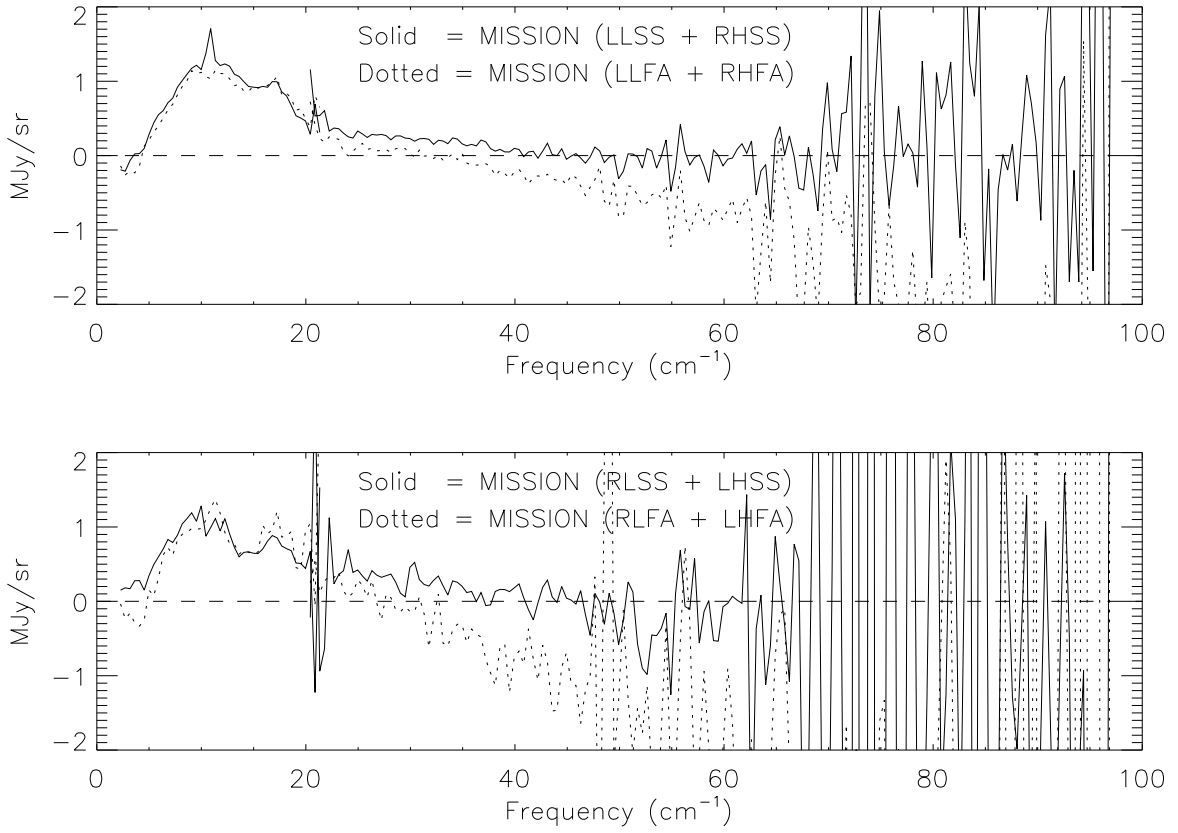Fig. 6.2.— '4K Horn' offset correction spectra — Applied to the observations for the 4 K horn period.

Fig. 6.3.— 'Mission' offset correction spectra — Applied to the observations for the entire mission.
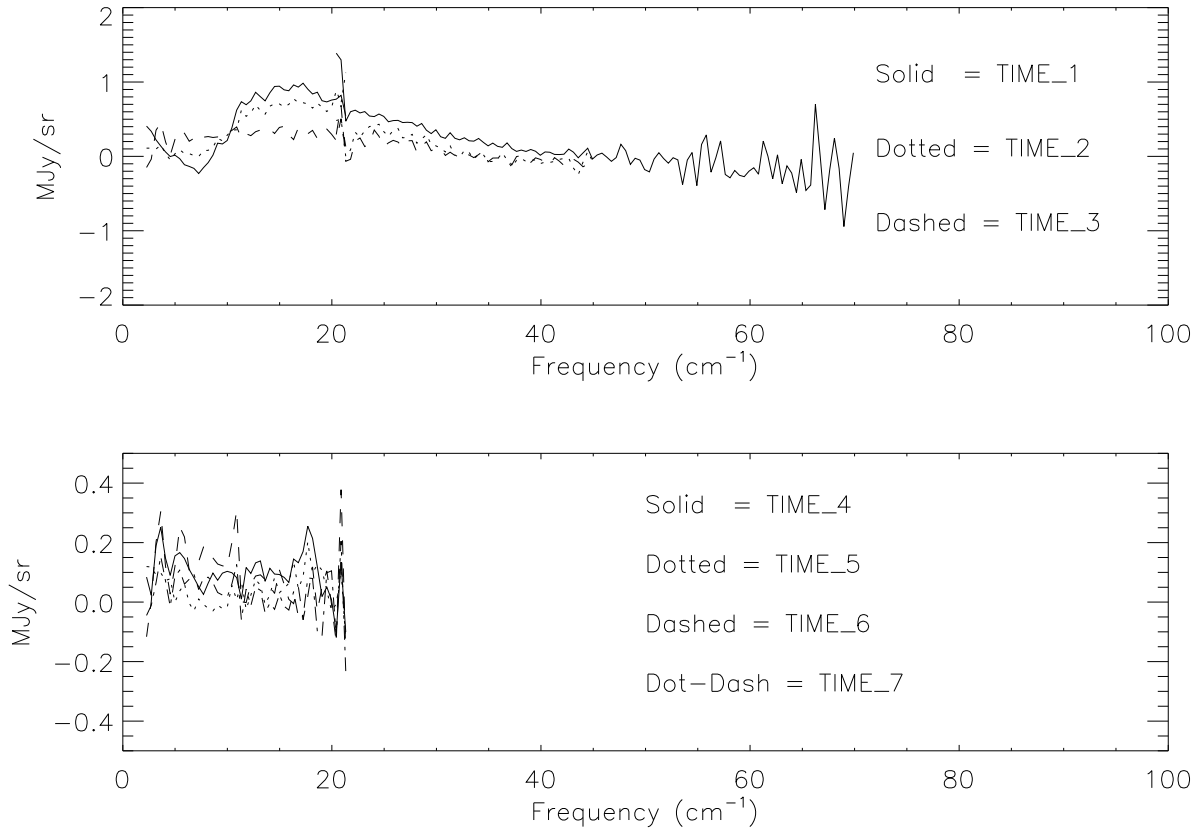
6.3.2. Time Functions

Fig. 6.4.— Time varying correction spectra — Based on Legengre polynomial stripe kernal

We have replaced the decaying exponentials of the previous destriper with Legendre polynomials for this destriper. This more general form is preferred for several reasons. The time constant for the decay is frequency-dependent. The previous selection of two time constants represented a best compromise among the frequencies. With our improved sensitivity, this selection was found to be inadequate. As we expanded the number of time constants, the selection of optimum values became cumbersome. Also, the non-orthogonality of the functions resulted in a poorly conditioned matrix inversion. The Legendre polynomials, defined so that they are orthogonal over the mission interval, eliminated inversion problems, eliminated the need to select time constants, and allowed for flexibility in destriping at different frequency bands by selecting an independent set of polynomial orders for each frequency band. The polynomial orders were determined by trial. For each frequency band, increasing orders of polynomials were tried until the

improvement in χ^2 became insignificant as measured by an F-statistic. The following sets of time functions were determined :

LOWF : [1,2,3,4,5,6,7]   HIF2 : [1,2,3]   HIF3 : [1]   HIF4 : None

The argument of the Legendre functions is defined to vary linearly with time from +1 at the beginning of the mission to -1 at the end to satisfy orthogonality. The DC term is not included in the set of time functions, because it is degenerate with the mission tophat function, as described above. Unlike the tophat functions, the time functions are derived in common for all of the channel combinations, under the assumption that a common source is being modelled.

6.3.3.   Source Gradient Functions

We compare observations grouped into the same sky pixel. Because of the finite sizes of the pixel and the *FIRAS* beam (Section 7.9.4), spatial gradients in the source spectra in the vicinity of the pixel will produce variations which are not intrinsic to the *FIRAS* instrument. Crosstalk between these variations and the model functions will introduce errors to the offset spectra, hereafter referred to as "stripes" . Previously, this source of error was handled by excluding data from pixels within 10° of the Galactic plane, under the assumption that spatial gradients at higher Galactic latitudes were negligibly small. For the final release, we have added model functions to account for the spatial gradients, enabling us to include more data in the destriper, and assuring that gradient errors at higher Galactic latitudes truly are suppressed.

The gradient functions were derived from the *DIRBE* data. First the high resolution *DIRBE* data were convolved with the *FIRAS* beam (Section 7.9.4) centered on each of the 6144 skycube pixels. Then a six parameter quadratic model was used to fit each pixel and its nearest eight neighbors. That model was used to estimate the *DIRBE* intensity for each coadd. Finally the weighted average of the coadd estimates for each pixel were subtracted from the estimates for that pixel. This was done so that there is no net signal in the model. Functions were formed from *DIRBE* bands 8, 9, and 10 (100, 140 and 240 μm) although only the functions for bands 9 and 10 were used in the released destriper models. F-statistic analysis indicated that two *DIRBE* gradient stripes were optimal. We selected the Band 10 and Band 9 functions.
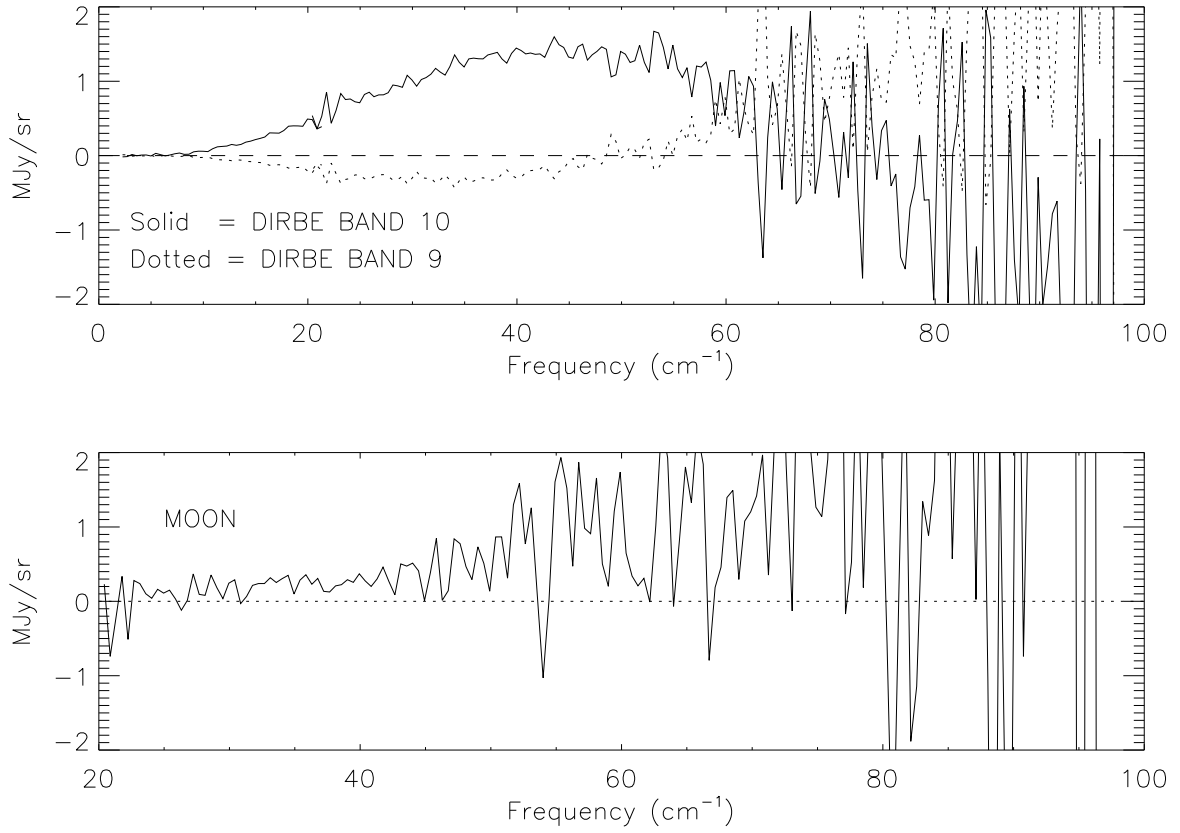
Fig. 6.5.— Sky gradient and moon contamination offset correction spectra — By construction the net contribution of the sky gradient to the pixel spectra is zero.

6.3.4. Moon Contamination

Since the beam profile is not ideal, there is some residual contamination from the Moon, even at angles greater than the 22° data quality cutoff. For the previous data release, we reported 3σ upper limits for the moon contamination. The improved sensitivity for this release has resulted in a detection of moon contamination. We have added a model function to allow the destriper to remove it by an offset correction.

For each sky observation, the moon angles and weights for its component interferograms were recovered, and the fraction of the coadd weight with moon angles within given ranges was computed. The residuals of the coadd spectra from the pixel mean were recovered from the results of the previous destriper runs, and examined as a function of observation weight at the various moon angles. Positive residuals were found for lower moon angles for all high channel frequency bands, indicating the presence of detectable moon contamination at frequencies greater than 600 GHz. The residuals were fit by a second order polynomial of moon angle to produce a simple but adequate model of moon contamination as a function of moon angle. This function was sufficiently similar for all high channel frequency bands that a single model was used for all bands. The moon contamination model function for each observation was then constructed as the weighted mean function of its component interferograms.

6.3.5. Dihedral Functions

Previous releases disqualified interferograms with associated dihedral temperatures greater than 3.5 ° K, eliminating a large amount of data taken during the first four months of the mission, when MTM power dissipation events caused dihedral heating spikes (Section 3). For this release, we have retrieved these data by grouping sky coadds by dihedral temperature. This advance was made possible by the use of interferograms from neighboring pixels in template formation, thereby allowing the formation of coaddable groups for each of six dihedral temperature ranges (Section 4.3) . Trial destriper runs showed that there were significant residuals correlated with dihedral temperature for this expanded set of sky data. The source of these residuals could be calibration errors in the dihedral emissivity and/or other instrumental effects associated with the MTM power dissipation. The residuals appeared to roughly fit a dependence on the square of the dihedral temperature. To correct for effects associated with dihedral heating events, we have constructed a function equal to the square of the dihedral temperature minus the square of the median dihedral temperature for all calibration observations used in the destriper. The use of the dihedral function was also determined by an F-statistic analysis.
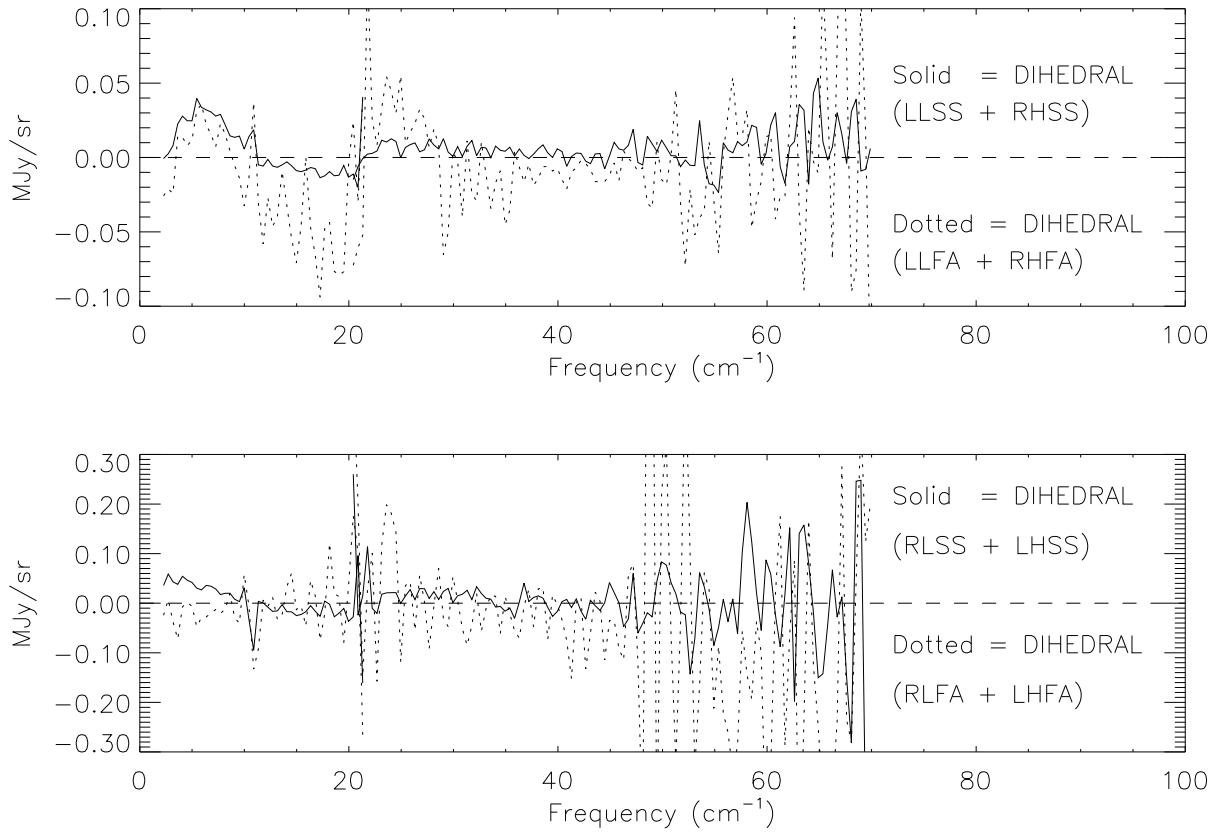
Fig. 6.6.— 'Dihedral' offset correction spectra — Based on a model where the correction is proportional to changes in the square of the dihedral temperature, relative to a nominal temperature.

LOWF : Yes   HIF2 : Yes   HIF3 : Yes   HIF4 : No

The definition of the function means that no dihedral correction is applied for observations with dihedral temperature equal to the reference temperature of 2.063 K. Dihedral effects at this temperature are absorbed into the mission stripes.
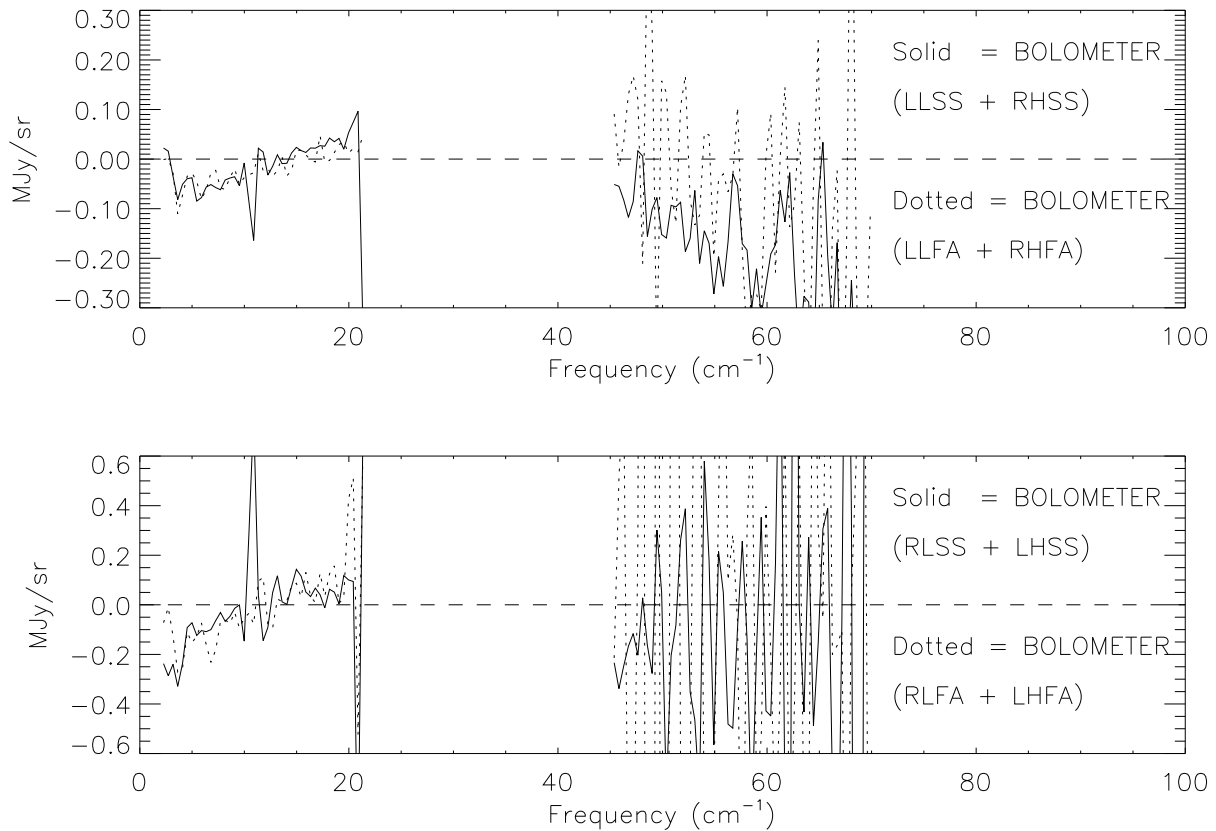
6.3.6. Bolometer Functions

Fig. 6.7.— 'Bolometer' offset correction spectra — Based on a model where the correction is proportional to changes in the bolometer responsivity, a function of the bolometer temperature and bias voltage, relative to a nominal responsivity.

Trial destriper runs also showed residuals correlated with bolometer temperature, as expressed by the derived bolometer responsivity (Section 5.3.2) . The correlation was

roughly linear with responsivity. A bolometer function was defined to be the deviation of responsivity from the mean, normalized by the RMS variation of responsivity. The bolometer function was used for those frequency bands for which the F-statistic indicated significant reduction in variance :

LOWF : Yes   HIF2 : No   HIF3 : Yes   HIF4 : No

The definition of the function means that no bolometer correction is applied for observations with responsivity equal to the reference values of -1.974, -1.6261 for the LL detector and RL detector respectively. The referance values for the LH and RH detectors are -.5235 and -.5607 in the slow scan mode and -.4919 and -.5312 in the fast scan mode. These were chosen as the median values of the responsivity. Bolometer effects at these responsivities are absorbed into the mission stripes.

6.3.7. Vibrations

Examination of the destriper residuals showed that the largest residuals were found at frequencies associated with major MTM resonances. These frequencies are at 318 GHz and 2203 GHz for slow scans, and at 212 GHz and 1469 GHz for fast scans (Sections 5.3.2 and 7.9.1). We correct for these by constructing a model function for the residual at each vibration frequency. Our model is an empirical time function derived by smoothing the observed residuals in time. The intent is to reduce the contribution from detector noise by averaging over a sufficiently large number of time-ordered observations so that the dominant remaining residual is due to vibration effects. We use weighted mean residuals for the observations nearest in time for each of the individual channel observations. The residuals have opposite signs for the left and right sides, so we treat the left channel data separately from the right channel data. This indicates a voltage effect rather than a photometric effect. It was also necessary to separate the fast scan data from the slow scan, as the vibration effects are at different frequencies for the different scan speeds.

For the vibration effect at 212 GHz, there was no excess variance in the residuals. No model function was constructed for this effect. For the vibration effect at 318 GHz, we averaged the residuals for the nearest 200 observations for LLSS and RLSS, setting the functions to zero for LLFA and RLFA. The function is called VIBRATION_10 . For the vibration effect at 1469 GHz, we averaged the residuals for the nearest 200 observations for LHFA and RHFA, setting the functions to zero for LHSS and RHSS. The function is called VIBRATION_49 . For the vibration effect at 2203 GHz, we averaged the residuals for the nearest 100 observations for LHSS and RHSS, setting the functions to zero for LHFA and
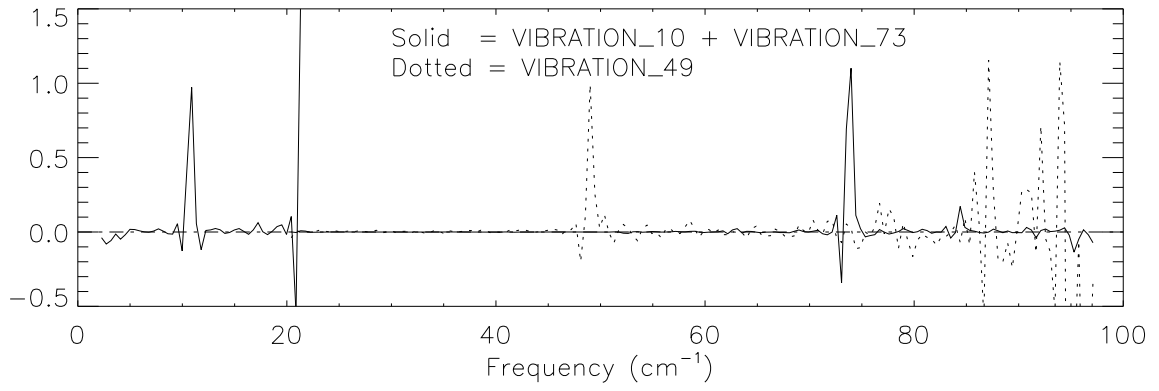
Fig. 6.8.— 'Vibration' offset correction spectra — Derived from a model proportional to the residual signal at the MTM resonaance frequencie.

RHFA. We were able to use a shorter time scale filter for this vibration because its relative effect was larger compared to the detector noise, thus requiring less averaging of the detector noise contribution to the residuals. The function is called VIBRATION_73 .

Examinations of the C-Vectors before and after destriping with the new vibration functions showed that the excess variances at 318 GHz and 1469 GHz were eliminated, as was about 85% of the excess variance at 2203 GHz. Evidence that we really were eliminating vibration effects was seen by the fact that the only features in the correction spectra were found at the vibration frequencies, at their harmonic frequencies, and at the beat frequencies between the 318 GHz and 2203 GHz vibrations. About 15% of the excess variance at 2203 GHz remained. We attempted to eliminate this by constructing a second model function for this vibration from the new residuals. The second function was also a smooth function of time constructed by fitting a 10th order Legendre function to the correlation function between the new residual spectra and the mean residual spectrum for a specified time range, chosen as the 6K horn interval. We found that the fitted model functions were anti-correlated for LHSS and RHSS, and uncorrelated for LHFA and RHFA, giving us confidence that we were modelling the 2203 GHz vibration effect. The function is called VIBRATION_73_X. Comparison of C-Vectors before and after destriping with the secondary vibration function showed that most of the remaining 15% extra variance was eliminated.

6.4.   Algorithmic Considerations

The least-squared fit model is linear, therefore in principle it can be solved through matrix inversion. However, because the pixel spectra are fit parameters, this matrix is quite large ($> 6000 \times 6000$) and a direct inversion is not practical. Fortunately, a large portion of the matrix is diagonal and can be inverted simply if partitioned. (We will henceforth call this the *curvature matrix* after Bevington (1969).)

If we write:

$$\mathbf{M} \equiv \begin{pmatrix} \mathbf{S} & \mathbf{R} \\ \mathbf{R^T} & \mathbf{D} \end{pmatrix} \tag{17}$$

where $\mathbf{S}$ is a square matrix with $\mathbf{S}_{km} = \sum_i f_{ki} w_i f_{mi}$, $\mathbf{R}$ is a rectangular matrix with $\mathbf{R}_{pk} = \sum_{i \in p} f_{ki} w_i$, and $\mathbf{D}$ is a diagonal matrix with $\mathbf{D}_{pp'} = \delta_{pp'} \sum_{i \in p} w_i$, then we can express its inverse as:

$$\mathbf{M^{-1}} = \begin{pmatrix} \mathbf{Q} & -\mathbf{QRD^{-1}} \\ -\mathbf{D^{-1}R^TQ} & \Upsilon \end{pmatrix} \tag{18}$$

where

$$\mathbf{Q} \equiv (\mathbf{S} - \mathbf{R}\mathbf{D}^{-1}\mathbf{R}^{\mathbf{T}})^{-1} \tag{19}$$

and

$$\mathbf{\Upsilon} \equiv \mathbf{D}^{-1} + \mathbf{D}^{-1}\mathbf{R}^{\mathbf{T}}\mathbf{Q}\mathbf{R}\mathbf{D}^{-1}. \tag{20}$$

Thus we see that the largest non-diagonal matrix that must be inverted is the $\mathbf{Q}$ matrix, whose maximum dimension is 30×30.

6.5. Destriper Project Data Sets

The derived quantities of the destriper fit are the correction offset spectra J_ν for each model function, hereafter referred to as "stripes", the spectra A_ν for each sky pixel, hereafter referred to as the "skymap" spectra, and the destriper errors. These quantities are included in the project data sets, as indicated in Table 6.1 . A description of the contents of these data sets can be found in Appendix G.

The A-Vector, C-Matrix, Pixel χ^2, and C-Vector are discussed in Chapter 7. The coadd ZODI model is discussed in Chapter 8. The coadd *DIRBE* gradient functions were discussed in Section 6.3. The orthogonalized and physical stripe errors are discussed in Chapter 7. The pixel ZODI model is the weighted mean of the coadd ZODI model. The ZODI models are included in the destriper data sets because the coadd ZODI spectra were removed prior to destriping. This was done to prevent time variability of the zodiacal light from affecting the destriper. After destriping, the ZODI was added back in to the spectra. The spectra in the FMD_SKY data set therefore include the zodiacal light.

The physical stripes, derived from the FMD_PST data sets, are presented in Figures 6.1 - 6.8. Figures derived from the FMD_AVC, FMD_CSQ, and FMD_CVC data sets will be presented in Chapter 7. The FITS headers for the FMD data sets are given in Appendix G.